A mouse-human phase 1 co-clinical trial of a protease-activated fluorescent probe for imaging cancer

HHS Public Access

Author manuscript

Sci Transl Med. Author manuscript; available in PMC 2017 January 06.

Published in final edited form as:

Sci Transl Med. 2016 January 6; 8(320): 320ra4. doi:10.1126/scitranslmed.aad0293.

A mouse-human phase 1 co-clinical trial of a protease-activated fluorescent probe for imaging cancer

Melodi Javid Whitley[1,2], **Diana M. Cardona**[3], **Alexander L. Lazarides**[4], **Ivan Spasojevic**[5,6], **Jorge M. Ferrer**[7], **Joan Cahill**[8], **Chang-Lung Lee**[8], **Matija Snuderl**[9,*], **Dan G. Blazer III**[10], **E. Shelley Hwang**[10], **Rachel A. Greenup**[10], **Paul J. Mosca**[10], **Jeffrey K. Mito**[1,2], **Kyle C. Cuneo**[8], **Nicole A. Larrier**[8], **Erin K. O'Reilly**[11], **Richard F. Riedel**[5], **William C. Eward**[12], **David B. Strasfeld**[7], **Dai Fukumura**[9], **Rakesh K. Jain**[9], **W. David Lee**[7], **Linda G. Griffith**[13], **Moungi G. Bawendi**[14], **David G. Kirsch**[1,8,†,‡], and **Brian E. Brigman**[12,‡]

[1]Department of Pharmacology and Cancer Biology, Duke University Medical Center, Durham, NC 27710, USA

[2]Medical Science Training Program, Duke University Medical Center, Durham, NC 27710, USA

[3]Department of Pathology, Duke University Medical Center, Durham, NC 27710, USA

[4]School of Medicine, Duke University Medical Center, Durham, NC 27710, USA

[†]Corresponding author. david.kirsch@duke.edu.
[*]Present address: Department of Pathology, NYU Langone Medical Center, New York, NY 10016, USA.
[‡]Co-senior authors.

SUPPLEMENTARY MATERIALS
www.sciencetranslationalmedicine.org/cgi/content/full/8/320/320ra4/DC1
Materials and Methods
Fig. S1. In vitro incubation of LUM015 with mouse tissues.
Fig. S2. The percentage of tumor cells that are $Cy5^+$ after administration of LUM015.
Fig. S3. In vivo detection of residual fluorescence within the mouse tumor bed.
Fig. S4. Summary pharmacokinetic data from mice and humans.
Fig. S5. Contribution of protease-activation and LUM015 distribution for tumor-selective fluorescence.
Table S1. No adverse pharmacological activity of LUM015 in humans.
Table S2. Liver function tests.
Table S3. Ex vivo imaging of human tissues.
Table S4. Correlating tissue fluorescence with metabolite concentration.
References (34–40)

Author contributions: M.J.W. participated in the design and execution of the clinical protocol, designed and performed experiments, analyzed and interpreted data, and wrote the manuscript. D.M.C., A.L.L., I.S., C.-L.L., M.S., and J.K.M. designed and performed experiments, analyzed and interpreted data, and contributed to the writing of the manuscript. J.M.F., D.B.S., W.D.L., L.G.G., and M.G.B. participated in the design of the clinical protocol, designed experiments, and analyzed and interpreted data. J.C. participated in the design of the clinical protocol, identified human subjects, and participated in sample procurement. D.G.B., E.S.H., R.A.G., and P.J.M. identified human subjects and participated in sample procurement. K.C.C., N.A.L., E.K.O., R.F.R., and W.C.E. participated in the design of the clinical protocol and edited the manuscript. E.K.O. drafted, submitted, and maintained the investigational new drug (IND) related to the phase 1 study. D.F. and R.K.J. analyzed and interpreted data and contributed to the writing of the manuscript. R.F.R. and B.E.B. served on the safety monitoring committee. D.G.K. participated in the design of the clinical protocol, held the IND, designed and oversaw the laboratory studies, interpreted the data, and wrote the manuscript. B.E.B. designed and supervised the clinical protocol, participated in sample procurement, and edited the manuscript.

Competing interests: W.D.L. is a cofounder and the CEO of Lumicell Inc., a company that is commercializing LUM015 and the LUM imaging system. M.G.B. is a cofounder of Lumicell Inc. and is a member of its scientific advisory board. L.G.G. and D.G.K. are members of the Lumicell Inc. scientific advisory board. W.D.L., M.G.B., and J.M.F. are co-inventors of LUM015 under U.S. patent application 20140301950. W.D.L., M.G.B., J.M.F., and D.G.K. are co-inventors of the handheld imaging device under U.S. patent 20140301950-A1.

Data and materials availability: LUM015 and LUM033 can be obtained from Lumicell Inc.

[5]Department of Medicine, Duke University Medical Center, Durham, NC 27710, USA

[6]PK/PD Core Laboratory, Duke Cancer Institute, Duke University Medical Center, Durham, NC 27710, USA

[7]Lumicell Inc., Wellesley, MA 02481, USA

[8]Department of Radiation Oncology, Duke University Medical Center, Durham, NC 27710, USA

[9]Edwin L. Steele Laboratory, Department of Radiation Oncology, Massachusetts General Hospital and Harvard Medical School, Boston, MA 02114, USA

[10]Department of Surgery, Duke University Medical Center, Durham, NC 27710, USA

[11]Duke Translational Medicine Institute, Regulatory Affairs Group, Duke University Medical Center, NC 27710, USA

[12]Department of Orthopaedic Surgery, Duke University Medical Center, Durham, NC 27710, USA

[13]Department of Biological Engineering, Massachusetts Institute of Technology, Cambridge, MA 02142, USA

[14]Department of Chemistry, Massachusetts Institute of Technology, Cambridge, MA 02142, USA

Abstract

Local recurrence is a common cause of treatment failure for patients with solid tumors. Intraoperative detection of microscopic residual cancer in the tumor bed could be used to decrease the risk of a positive surgical margin, reduce rates of reexcision, and tailor adjuvant therapy. We used a protease-activated fluorescent imaging probe, LUM015, to detect cancer in vivo in a mouse model of soft tissue sarcoma (STS) and ex vivo in a first-in-human phase 1 clinical trial. In mice, intravenous injection of LUM015 labeled tumor cells, and residual fluorescence within the tumor bed predicted local recurrence. In 15 patients with STS or breast cancer, intravenous injection of LUM015 before surgery was well tolerated. Imaging of resected human tissues showed that fluorescence from tumor was significantly higher than fluorescence from normal tissues. LUM015 biodistribution, pharmacokinetic profiles, and metabolism were similar in mouse and human subjects. Tissue concentrations of LUM015 and its metabolites, including fluorescently labeled lysine, demonstrated that LUM015 is selectively distributed to tumors where it is activated by proteases. Experiments in mice with a constitutively active PEGylated fluorescent imaging probe support a model where tumor-selective probe distribution is a determinant of increased fluorescence in cancer. These co-clinical studies suggest that the tumor specificity of protease-activated imaging probes, such as LUM015, is dependent on both biodistribution and enzyme activity. Our first-in-human data support future clinical trials of LUM015 and other protease-sensitive probes.

INTRODUCTION

Surgical resection is the primary treatment modality for most solid tumors diagnosed before metastatic spread. In patients with soft tissue sarcoma (STS) of the extremity and breast cancer, organ-sparing surgery alone prevents local recurrence in about two-thirds of patients (1–3). Local recurrence is due to residual cancer in the tumor bed, the risk of which is

inferred by histopathological evaluation for the presence of tumor cells on the surface of the excised margin (1, 4). Intraoperative frozen margin assessment is limited by time and prone to sampling error, leading to false-negative results in up to 23% of cases (5). An intraoperative technique to accurately identify microscopic residual disease within the tumor bed could be used to decrease the risk of a positive surgical margin, reduce the rate of re-resection, and tailor adjuvant therapy.

Emerging approaches to detect microscopic residual disease within the tumor bed include spectroscopy and optical imaging. Raman spectroscopy measures the scattering properties of tissues, and tumor-targeted Raman reporters like gold nanostars can provide excellent tumor-to-normal tissue contrast (6, 7). Fluorescence optical imaging resolves molecular features, and nonspecific fluorescent imaging probes such as methylene blue and indocyanine green provide contrast between tumor and normal tissues and are currently in clinical trials. The mean tumor-to-background ratio (TBR) with these imaging agents ranges from 1.2 to 8.5 in mouse and human studies (8–10). To increase the TBR, targeted (11–13) and activatable fluorescent probes have also been developed. Activatable probes are optically silent until cleaved by proteases that are overexpressed by tumors, such as cathepsin proteases (14–16). In a previous study, we used the *LSL-Kras*$^{G12D/+}$*; p53*$^{flox/flox}$ (KP) and *Braf*$^{Ca/+}$; *p53*$^{flox/flox}$ (BP) mouse models of STS and a wide field-of-view imaging system to detect cathepsin-activated fluorescence in tumor cells (17). Residual fluorescence in the tumor bed correlated with local recurrence, and image-guided surgery improved outcomes for mice. This intraoperative imaging system has also been used in canine patients with spontaneous tumors (18).

Although protease-activated probes have shown promise preclinically, translation has been hindered by suboptimal preclinical models and limited funding for probe synthesis, toxicity studies, and phase 1 clinical trials. We were able to overcome these hurdles, among others, to translate protease-activated probes into the operating room. Here, we specifically explored the use of LUM015, a novel PEGylated protease-activated far-red fluorescent imaging probe. Preclinical toxicity studies of LUM015 were performed in rats and indicated a wide margin of safety. We report here a first-in-human phase 1 trial of LUM015 to test the safety of the probe in patients undergoing surgery for STS and breast cancer as well as LUM015 pharmacokinetics. Co-clinical studies in mice were conducted to optimize the dose and timing of LUM015 administration and to investigate the in vivo mechanisms of tumor specificity. Our studies support further clinical development of LUM015 in clinical trials with intraoperative imaging of the tumor bed.

RESULTS

LUM015 forms two different optically active metabolites

LUM015 consists of a commercially available fluorescence quencher molecule (QSY21) attached through a GGRK peptide to a 20-kD polyethylene glycol (PEG) and a Cy5 fluorophore (Fig. 1A). LUM015 is optically inactive, but upon proteolytic cleavage by cathepsins K, L, and S (and, to some extent, B), the quencher is released (fragment 1) to create the optically active fragment 2 (Fig. 1B). Additional cleavage of LUM015 or fragment 2 yields the optically active fragment 3 (Fig. 1A). High-performance liquid

chromatography (HPLC) revealed distinct peaks for fragments 2 and 3 (Fig. 1C). The low-level fluorescence detected from LUM015 itself is from ~1% Cy5 fluorescence not absorbed by the quencher. Patient plasma samples showed a strong peak corresponding to fragment 3 as well as a smaller peak representing fragment 2 and uncleaved LUM015 (Fig. 1D), and human plasma profiles showed fragment 3 levels increasing during the first 8 hours after injection followed by clearance at a slower rate (Fig. 1E).

We then injected mice with and without primary STS tumors with LUM015 and measured $[\text{fragment 3}]_{\text{plasma}}$ over time after administration. At 1 hour, the concentration of fragment 3 in plasma peaked in mice with tumors, but by 2 hours, plasma levels were similar to mice with no tumor, suggesting that fragment 3 was appreciably produced in nontumor tissues (Fig. 1F). In tumor tissue, most of LUM015 was metabolized, whereas in blood, muscle, liver, and kidney tissue, half or more of LUM015 remained uncleaved (fig. S1). In contrast to fragment 3 being the major metabolite after in vivo administration of LUM015 to patients, fragment 2 was the predominant cleavage product in vitro.

LUM015 fluorescently labels tumor cells in mice

To test the specificity of LUM015 for tumor cells, we administered LUM015 (3.5 mg/kg) via tail vein injection into 16 mice with primary STS in the lower extremity. This dose of LUM015 was chosen on the basis of preclinical studies performed with other protease-activatable probes in the same mouse model (17). Six hours later, we resected the STS and normal muscle from the contralateral leg. Fluorescence imaging of the resected tissues revealed a mean tumor fluorescence that was nearly fivefold higher than that of muscle (Fig. 2A). In a mouse model of breast cancer, LUM015 fluorescence was significantly greater in tumor than in muscle (Fig. 2B).

Because tumors consist of cancer and stromal cells, we next investigated to what extent LUM015 labeled these cells using mice with tumors that express yellow fluorescent protein (YFP). After 6 hours, tumors resected from mice injected with LUM015 had a significantly higher proportion of $Cy5^+$ fluorescent cells compared to control animals given saline (Fig. 2C). About 62% of the LUM015-labeled cells were YFP^+ tumor cells, and less than 10% were $CD11b^+$ tumor-associated monocytes and macrophages (Fig. 2C), indicating that most Cy5-labeled cells were tumor cells. Polymerase chain reaction (PCR) genotyping of genomic DNA from the $Cy5^+$ cells that were $YFP^-/CD11b^-$ revealed that most of these cells were tumor cells, which activated LUM015 but may have lost expression of the YFP marker, mixed together with some $CD11b^-$ stromal cells (fig. S2A). Conversely, in pure populations of $YFP^+/CD11b^+$ cells, the proportion of $Cy5^+$ cells was higher in the tumor cell population than in the monocyte population, but the efficiency of labeling in tumor cells was about 20% in mice (fig. S2).

Having demonstrated that LUM015 fluorescently labels sarcoma cells, we next used an autochthonous mouse model of STS with marginal resection to determine if residual fluorescence in the tumor bed after surgical removal of the tumor predicted local recurrence. Residual fluorescence within the tumor bed was determined intraoperatively as fluorescence exceeding 80% of the minimum signal from the excised tumor (fig. S3) (17). After imaging the tumor bed, the surgical wound was closed, and the mice were monitored for local

recurrence–free survival. All mice positive for residual fluorescence at the time of surgery developed local recurrence of their tumors within 70 days of surgery. In comparison, only one-third of the mice without residual fluorescence in the tumor bed experienced local recurrence within 200 total days of follow-up (Fig. 2D).

LUM015 is safe in humans

After demonstrating that LUM015 selectively labeled sarcoma and breast cancer in mice, we performed a first-in-human phase 1 clinical trial of LUM015. This trial enrolled 15 patients, 12 with STS and 3 with invasive ductal carcinoma (IDC) of the breast. Four of the 12 STS patients had undifferentiated pleomorphic sarcoma (UPS), and the other eight represented several different STS subtypes. The tumor subtypes, grade, size, and anatomic locations are described in Table 1. LUM015 was administered to six patients at a 0.5 mg/kg dose, six patients at a 1.0 mg/kg dose, and three patients at a 1.5 mg/kg dose, according to a modified 3 + 3 design (NCT01626066). These human doses were chosen on the basis of the estimated effective dose of 3.5 mg/kg in mice, which often corresponds to a lower effective dose in humans owing to differences in the ratio of body surface area to body weight (19). Surgical removal of the tumors immediately followed by ex vivo fluorescence imaging of the resected specimens was done either the same day as probe injection (at ~6 hours) or the following day (at ~30 hours). Tissue samples imaged ex vivo were biopsied for subsequent histological analysis.

LUM015 was well tolerated by study subjects, and no adverse pharmacological activity or hypersensitivity reactions occurred during the study (table S1). All subjects experienced green chromaturia, which was expected based on the blue color of LUM015. Two sarcoma patients had wound healing complications, which is within the expected range for this patient population and not considered related to LUM015; both of these patients had received preoperative radiation therapy, which is known to delay wound healing in STS patients (20). Patient 11 experienced a minor transient elevation of liver function tests for aspartate aminotransferase at 59 U/liter (normal range, 15 to 41) and alanine transaminase at 58 mg/dl (normal female range, 14 to 54) 8 hours after LUM015 administration, which was determined to be only possibly related to the investigational probe and therefore did not meet the criteria for adverse pharmacological activity, as defined by the clinical protocol (table S2). Notably, the tissue imaged for patient 10 did not include tumor, and therefore, this patient was excluded from tumor tissue analyses.

Co-clinical studies in mice and humans show similar pharmacokinetics

Blood samples were collected from mice and patients at regular intervals after intravenous administration of LUM015, and liquid chromatography–tandem mass spectrometry (LC-MS/MS) was used to measure $[LUM015]_{plasma}$ at these time points. Summary pharmacokinetic parameters suggesting a linear dose response in humans are reported in fig. S4. Plasma clearance profiles for mice and humans injected with a 1.5 mg/kg dose of LUM015 were similar (Fig. 3A). Tumor fluorescence in the first six humans imaged at 30 hours was lower than fluorescence measured in mice at 6 hours, but in both mice and humans, absolute tumor fluorescence was significantly higher when measured 6 hours after LUM015 administration compared to 30 hours (Fig. 3B). In contrast, we did not find a

significant effect of imaging time on the tumor-to-normal tissue fluorescence ratio (T/N) in humans or mice (Fig. 3C). Thus, the imaging time point was shortened to 6 hours after LUM015 administration for the remainder of the phase 1 trial. Furthermore, at 6 hours, the fluorescence ratio (tumor/normal) measured in humans administered the highest LUM015 dose (1.5 mg/kg) was significantly higher than those measured in the two lower-dose cohorts (Fig. 3D).

LUM015 fluorescence is tumor-selective in STS and breast cancer patients

To determine if preoperative administration of LUM015 results in tumor-specific fluorescence, we compared the absolute fluorescence in the tumor with the absolute fluorescence in adjacent normal tissue from all patients (Table 1), except for patient 10. The presence or absence of cancer in the samples was confirmed by subsequent histological analysis by a pathologist blinded to the imaging data (table S3). Normal muscle, adipose, or breast tissue from the margin of tissue resected around the tumor was used for the normal tissue comparison unless otherwise noted in table S3. Three representative examples of ex vivo imaging from a patient with a high-grade UPS of the thigh, a patient with a high-grade myxofibrosarcoma of the thigh, and a patient with a high-grade IDC of the breast are shown (Fig. 4, A to C). UPS is the most common type of STS in the trial and is phenotypically most similar to the mouse model in our preclinical studies. Myxofibrosarcoma is locally aggressive, and complete resections are challenging; thus, these patients may particularly benefit from this intraoperative imaging technology.

For each patient, we imaged one to six tumor and normal tissue sites that were histologically confirmed, and the mean fluorescence value is reported. Overall, tumor fluorescence was significantly higher than matched normal tissue fluorescence with a mean tumor/normal fluorescence ratio of 4.1 (Fig. 4D). The tumor/normal fluorescence ratio was less than or equal to 1 in two of the patients, both of whom were imaged at the 30-hour imaging time point and had low-grade sarcomas (well-differentiated liposarcoma and myxoinflammatory fibroblastic sarcoma/hemosiderotic fibrolipomatous tumor). Furthermore, we found that across all patients, the means of absolute tumor, muscle, and adipose fluorescence values were significantly different (Fig. 4E).

Biodistribution and protease activation contribute to tumor fluorescence

After determining that fragment 3—with Cy5, no PEG— was the major LUM015 metabolite in human plasma (Fig. 1), we measured the concentrations of both fragments and intact LUM015 in human tissues (table S4) and in a cohort of 18 mice injected with LUM015 (1.5 mg/kg). At 6 hours, $[\text{fragment 3}]_{\text{tumor}}$ correlated significantly with tumor fluorescence in mice and in humans (Fig. 5A). A similar analysis of fragment 2 showed a weaker correlation with tissue fluorescence (Fig. 5A). To measure the contribution of proteolytic probe activation to tumor-selective fluorescence, we calculated the fraction of LUM015 and its metabolites that were present in the optically active state for each mouse sample. In the mouse cohort, sarcomas had a fraction of activated probe (FAP) of 0.38, which was about 50% higher than normal muscle (Fig. 5B). In human tumor samples imaged at 6 hours, tumors had a FAP of 0.26, which was about 60% higher compared to normal tissues (Fig. 5B), but this difference did not reach statistical significance, even at 30 hours.

In the mouse STS cohort and the human STS patients imaged at 6 hours with normal muscle available for comparison (patients 8, 11, 12, 13, and 14; table S3), tumor/muscle fluorescence ratios were correlated with the corresponding activation ratio; however, this correlation was significant only for the mouse samples (Fig. 5C). In an analysis inclusive of all patients, there was a significant correlation between fluorescence and activation (fig. S5A). To measure the contribution of biodistribution to tumor-selective fluorescence, the total concentration of LUM015 and its cleavage products, [total probe (TP)], was determined for each sample. In both the mouse and human STS cohorts, sarcomas had a [TP] that was greater than normal muscle (Fig. 5D). Additionally, [TP] was higher in human tumors imaged at 6 hours when compared to tumors imaged at 30 hours (fig. S5B). Furthermore, we found that tissue fluorescence and [TP] had a significant positive correlation in the mouse cohort, the human STS cohort, and the overall human data set (Fig. 5, E and F).

To image tumors with a probe that does not require protease activation, we injected STS-bearing mice with either LUM015 or LUM033, a constitutively active fluorescent imaging probe identical to fragment 2 (also from Lumicell Inc.). Six hours after injection, resected tumors had a tumor/normal fluorescence ratio twofold higher for LUM015 than for LUM033 (Fig. 5G). Therefore, protease activation may serve to double the level of tumor-to-normal contrast that is achieved by tumor-selective biodistribution alone. These findings suggest that tumor-selective distribution of LUM015 is a critical determinant of T/N, which is further enhanced by tumor-specific protease activation.

Because biodistribution is one of two major determinants of tumor-specific fluorescence measured after administration of LUM015, we used immunofluorescence and immunohistochemistry to further examine the distribution of LUM015 to tumor and normal tissues. As a control for immunofluorescence, we used formalin-fixed paraffin-embedded (FFPE) sections of tumor tissue from human sarcoma patients not injected with LUM015. Patients who had been injected with LUM015 showed a positive signal for PEG, whereas the control tissues did not (Fig. 6A). In a breast cancer sample from patient 15 that contained both areas of tumor and adjacent normal tissue, PEG signal localized to areas of tumor, with less intense staining in normal tissue (Fig. 6B). Areas adjacent to tumor containing a lymphocytic infiltrate were also negative for PEG staining. The amount of PEG staining was significantly less in normal muscle and breast tissues compared to sarcomas and breast cancer, respectively (Fig. 6, C and D). These results for PEG staining, together with the quantification of LUM015 and its metabolites, suggest that tumor-selective distribution of LUM015 may serve to delineate the tumor margin while protease activation intensifies the contrast between tumor and normal tissue types for intraoperative imaging.

DISCUSSION

There is an unmet need for a real-time method to determine the presence of microscopic residual cancer within the tumor bed at the time of surgery, which could reduce the need for re-resection, lower the rates of local recurrence, and personalize adjuvant therapy. A particularly attractive approach to detect residual disease is fluorescence imaging because it can be functionally and/or molecularly targeted and provide cellular resolution with

penetration depths of up to several millimeters (11). Protease-activated fluorescent imaging probes were first introduced more than 15 years ago to provide optical contrast between tumor and normal tissues (14, 21–23). Many of these probes have been tested in preclinical models. This is the first study to use these probes to image human cancers and investigate the relative importance of protease activation versus biodistribution for achieving tumor-to-normal tissue contrast.

We show here that the PEGylated, protease-activated probe LUM015 specifically labels tumors in a mouse model of STS as well as in humans with STS and breast cancer. Flow cytometric studies of tumors from LUM015-injected mice showed that most fluorescently labeled cells were tumor cells, and less than 1/10 were tumor-associated monocytes and macrophages. The labeling of tumor-associated macrophages likely occurs because these cells also express high levels of proteases (24), and the intraoperative identification and removal of these cells may, in fact, be beneficial to patients because these cells are associated with tumor progression and metastasis (25, 26). In mice injected with LUM015, residual fluorescence within the tumor bed was highly predictive of local recurrence, suggesting that this intraoperative imaging system could be useful to guide surgery and tailor adjuvant therapy.

In a first-in-human phase 1 trial in patients undergoing surgical resection of STS or breast cancer, we found that LUM015 is safe and well-tolerated at a dose that allows for detection of tumor-specific fluorescence. We observed that the plasma clearance profile of LUM015 in humans and mice is similar. On the basis of allometric scaling, we expected that the clearance rate would be significantly slower in humans (27, 28) so that a greater interval of time between LUM015 administration and tumor resection would be required to allow for optimal tumor-to-normal tissue contrast. Our results are consistent with the findings that standard allometric scaling does not accurately predict human pharmacokinetic parameters for PEGylated compounds (29). On the basis of this information, we modified the phase 1 clinical trial to include imaging at the 6-hour time point, resulting in higher tumor fluorescence in human cancers than imaging at 30 hours.

Consistent with data from mice and dogs (18), when patients with STS or breast cancer were injected with LUM015 before surgery, we found tumor tissue fluorescence measured ex vivo to be significantly higher than fluorescence measured from adjacent normal tissues. It is important to note that this study included patients with both sarcoma and breast cancer, and that within these tumors, different subtypes were included. A T/N of greater than 1 was measured in 12 of 14 patients, indicating that LUM015 may be effective for fluorescent labeling of many different types of cancer. However, the human T/N reported in this study were measured in ex vivo bulk tissue, and future clinical trials with LUM015 with in vivo tumor bed imaging will be necessary to define a clinically meaningful T/N cutoff. Nevertheless, the in vivo tumor bed imaging in our mouse experiments suggests that LUM015 can provide a sufficient T/N for detecting residual cancer.

Tissue measurements of LUM015, PEG, and its metabolites showed that selective biodistribution in tumors was an important factor in tumor-selective imaging. Tumor-specific protease activation serves to enhance the contrast that is established with differential

distribution, suggesting that by targeting the tumor through both mechanisms simultaneously, a larger tumor-to-normal contrast is achieved. However, in mice, we found that the generation of fragments in vivo did not require the presence of cancer and could be formed in isolated blood, muscle, liver, and kidney. This suggests that protease activation does not fully account for the tumor/normal ratio, and instead is established in part by tumor-selective accumulation through the enhanced permeability and retention effect.

This study shows that preoperative administration of LUM015 to patients with sarcoma or breast cancer results in tumor-specific fluorescence that can be detected upon ex vivo imaging of resected tissues. However, future clinical studies will be needed to measure fluorescence in vivo, specifically residual cancer cells at the tumor margins. We report in vivo imaging data from mice and show that intraoperative imaging with LUM015 predicts local recurrence with high specificity. However, some mice with negative residual fluorescence did develop local recurrence. Therefore, it will be necessary to optimize fluorescence thresholding methods to increase the sensitivity of the system while maintaining high specificity.

This work presents a first-in-human phase 1 clinical trial of an intravenously administered, protease-activated fluorescent intraoperative imaging probe. We have shown that LUM015 is safe for use in humans and generates tumor-specific fluorescence. These studies support future clinical trials of LUM015 using intraoperative imaging of the tumor bed and comparing imaging results with histopathology. A feasibility study of intraoperative imaging with the LUM system has recently started for breast cancer patients (NCT02438358), but it may be possible to use the probe for patients with other cancers, such as sarcoma (as demonstrated in mice) and gastrointestinal cancers. Our co-clinical studies in mice and humans reveal that pharmacokinetic and pharmacodynamic parameters are conserved across species, which may aid in the translation of other preclinical imaging agents for human use.

MATERIALS AND METHODS

Co-clinical study design

In this co-clinical study, data regarding the pharmacokinetics, specificity, and mechanism of action of LUM015 were gathered in both mice and humans. Preclinical studies in the mice provided justification for a phase 1 clinical trial in humans. During the clinical trial, parallel mouse studies were conducted to further explore clinical observations regarding LUM015 pharmacokinetics and the mechanism of tumor-selective fluorescence. The objective of the controlled laboratory experiments was to use a primary mouse model of STS and orthotopic models of breast cancer to investigate the in vivo activity of LUM015 and explore the mechanism of LUM015 distribution and activation in vivo.

All animal studies were performed in accordance with protocols approved by the Duke University and Massachusetts General Hospital Institutional Animal Care and Use Committees. Sample sizes were selected before initiating the study based on previous intraoperative imaging studies conducted in the laboratory (17), and power calculations were performed as described previously (30). Data collection was stopped if a smaller sample size achieved statistical significance. No outliers were excluded in this study. The mice in this

study were not randomized to their treatments and were selected on the basis of availability. The investigators were not blinded when performing tissue fluorescence measurements.

The primary objective of the single institution, open-label, nonrandomized phase 1 trial (NCT01626066) was to determine a safe and recommended dose of LUM015 that labels tumors. Secondary objectives included obtaining ex vivo imaging information of the tumor and any adjacent normal tissue as well as collecting pharmacokinetic/pharmacodynamic information. Patients with the diagnosis of STS or breast cancer scheduled for tumor resection were included. Patients treated with neoadjuvant radiation therapy were included in the study based on our previous data that radiation therapy does not alter the fluorescence from protease-activated imaging probes in a mouse model of STS (31). The sample size was determined on the basis of a modified 3 + 3 dose escalation design to provide information on the relationship between dose and fluorescence signal while observing patients for adverse pharmacological activity. No outliers were excluded in this study. Informed consent was obtained from each patient, and the study was approved by the Duke University School of Medicine and Copernicus Institutional Review Boards. The study was also run under an Investigational New Drug application filed with the U.S. Food and Drug Administration. A safety monitoring committee was formed to protect the rights, safety, and welfare of participants, and additional monitoring was done by the Duke Cancer Institute (DCI) Safety Oversight Committee.

Patients underwent standard operative and perioperative treatment. Resected patient tissues underwent standard surgical pathology procedures before being imaged and sampled for the study with the guidance of a clinical pathologist blinded to the fluorescence imaging measurements. Safety evaluations, described in Supplementary Materials and Methods, were conducted before and after peripheral intravenous administration of LUM015 at three predetermined doses: 0.5, 1.0, or 1.5 mg/kg. LUM015 was administered either the day before or on the morning of surgery. LUM015 was supplied free of charge from Lumicell Inc. Patient blood samples were collected before and after LUM015 administration for pharmacokinetic/pharmacodynamic studies.

Fluorescent agent administration and imaging

Mice were administered LUM015 or LUM033 via tail vein injection when tumors reached about 1000 mm^3 (4 to 5 mm in diameter). Blood samples for pharmacokinetic studies were obtained from the submandibular vein. After a specified time interval, the animals were euthanized, and tissues were removed for fluorescence imaging and other analyses. For the local recurrence study, tumors were removed and intraoperative assessment of residual fluorescence was performed as described previously (17). The handheld LUM imaging device was described previously (17), and the specifications are provided in Supplementary Materials and Methods. Normal and tumor tissues were identified grossly, and the imaging tip was applied to the tissue to obtain two to three images of the same location. The tissue was biopsied at the site of imaging for identification of the tissue type by histological analysis (H&E) and measurement of LUM015 and its metabolites (fragment 2 and Cy5-Lys).

Image processing was performed using a custom script developed in the Matlab programming environment (MathWorks) using standard corrections for background and signal distribution (32), described in Supplementary Materials and Methods. Mean pixel intensities derived from the Matlab script are reported in this study. For visual representation of images, the contrast and brightness of images were adjusted as described previously (17) so that the reader can appreciate the differences in fluorescence intensities between tumor and normal tissue.

Histological analysis, immunohistochemistry, and immunofluorescence

FFPE sample tissues were sectioned to create 5-μm-thick slides for H&E staining, PEG immunohistochemistry, and immunofluorescence studies. Staining and quantification methods are described in Supplementary Materials and Methods. Slides were reviewed by a clinical pathologist specializing in STS (D.M.C.), who was blinded to tissue fluorescence measurements.

Flow cytometry

KPY mice harboring primary sarcomas were injected with either LUM015 (3.5 mg/kg) or PBS vehicle, and tumors were collected 6 hours after injection. Cells were dissociated from tumors according to methods described previously (33). Total cells dissociated from tumors were incubated with rat anti-mouse CD16/32 immunoglobulin G (IgG) (BD Pharmingen) and phycoerythrin-Cy5–conjugated anti-mouse CD11b IgG (eBioscience). Data were collected from at least 200,000 cells by FACSCanto (BD Pharmingen) and analyzed by FlowJo (Tree Star Inc.). Genomic PCR analysis to show recombination of the mutant *Kras* allele was performed with the following primers: (i) 5′-GTCTTTCCCCAGCACAGTGC-3′; (ii) 5′-CTCTTGCCTACGCCACCAGCTC-3′; (iii) 5′-AGCTAGCCACCATGGCTTGAGTAAGTCTGCA-3′. The wild-type *Kras* allele yields a 622-bp band, the unrecombined *LSL-Kras*^{G12D} allele yields a 500-bp band, and the recombined 1-loxP-*Kras*^{G12D} allele yields a 650-bp band.

Plasma and tissue metabolite measurements

Concentrations of LUM015 and its metabolites in plasma and tissue samples were determined using LC-MS/MS as well as HPLC with fluorescence detection (HPLC-FD). A detailed methodology is presented in Supplementary Materials and Methods.

Statistics

Results are presented as means ± SEM unless otherwise indicated. Before analysis, all data were displayed graphically to determine whether parametric or nonparametric tests should be used. Two-tailed Student's *t* test was performed to compare the means of two groups, and a matched pair *t* test was used when comparing fluorescent measurements from the same patient. A Mann-Whitney test was performed to compare the means of two groups when data were distributed nonparametrically. Two-way ANOVA was performed to examine the interaction between two independent variables such as dose and imaging time, and one-way ANOVA was used when measuring the effect of only one variable, such as tissue type. These were followed by Bonferroni or Tukey's post hoc multiple comparison tests for

pairwise comparisons of individual treatments or tissue types. For local recurrence studies, Kaplan-Meier analysis was performed with the log-rank test for statistical significance. To find the correlation of two different measurements from the same sample, we determined the Pearson coefficient (r) and r^2. Significance was assumed at $P < 0.05$. All calculations were performed using Prism 6 (GraphPad).

Supplementary Material

Refer to Web version on PubMed Central for supplementary material.

Acknowledgments

We thank Y. Ma, N. Williams, and L. Luo for valuable assistance with histology, animal/human tissue imaging, and mouse colony management, respectively. We thank J. Kahn for her technical assistance with the mice in the breast cancer studies. We thank P. O'Donnell of the University of Kentucky, F. Hornicek of the Massachusetts General Hospital, S. Yoon of the Memorial Sloan Kettering Cancer Center, and R. Noveck of Duke University for serving on the patient safety committee for the phase 1 study. We thank B. Peterson for guidance on statistical design of the clinical trial.

Funding: Supported in part by the American Society of Clinical Oncology Advanced Clinical Research Award (D.G.K.), NIH T32 grant #T32GM007171 (M.J.W. and J.K.M.), National Cancer Institute Small Business Innovation Research award #1U43CA165024 (W.D.L.), National Center for Advancing Translational Science of the NIH grant #UL1TR001117 (E.K.O.), and Duke Comprehensive Cancer Center Support Grant 5P30-CA-014236-38.

REFERENCES AND NOTES

1. Pisters PW, Leung DH, Woodruff J, Shi W, Brennan MF. Analysis of prognostic factors in 1,041 patients with localized soft tissue sarcomas of the extremities. J Clin Oncol. 1996; 14:1679–1689. [PubMed: 8622088]
2. Fisher B, Anderson S, Bryant J, Margolese RG, Deutsch M, Fisher ER, Jeong JH, Wolmark N. Twenty-year follow-up of a randomized trial comparing total mastectomy, lumpectomy, and lumpectomy plus irradiation for the treatment of invasive breast cancer. N Engl J Med. 2002; 347:1233–1241. [PubMed: 12393820]
3. Yang JC, Chang AE, Baker AR, Sindelar WF, Danforth DN, Topalian SL, DeLaney T, Glatstein E, Steinberg SM, Merino MJ, Rosenberg SA. Randomized prospective study of the benefit of adjuvant radiation therapy in the treatment of soft tissue sarcomas of the extremity. J Clin Oncol. 1998; 16:197–203. [PubMed: 9440743]
4. Anscher MS, Jones P, Prosnitz LR, Blackstock W, Hebert M, Reddick R, Tucker A, Dodge R, Leight G Jr, Iglehart JD, et al. Local failure and margin status in early-stage breast carcinoma treated with conservation surgery and radiation therapy. Ann Surg. 1993; 218:22–28. [PubMed: 8328825]
5. Cendán JC, Coco D, Copeland EM III. Accuracy of intraoperative frozen-section analysis of breast cancer lumpectomy-bed margins. J Am Coll Surg. 2005; 201:194–198. [PubMed: 16038815]
6. Harmsen S, Huang R, Wall MA, Karabeber H, Samii JM, Spaliviero M, White JR, Monette S, O'Connor R, Pitter KL, Sastra SA, Saborowski M, Holland EC, Singer S, Olive KP, Lowe SW, Blasberg RG, Kircher MF. Surface-enhanced resonance Raman scattering nanostars for high-precision cancer imaging. Sci Transl Med. 2015; 7:271ra7.
7. Liu Y, Ashton JR, Moding EJ, Yuan H, Register JK, Fales AM, Choi J, Whitley MJ, Zhao X, Qi Y, Ma Y, Vaidyanathan G, Zalutsky MR, Kirsch DG, Badea CT, Vo-Dinh T. A plasmonic gold nanostar theranostic probe for in vivo tumor imaging and photothermal therapy. Theranostics. 2015; 5:946–960. [PubMed: 26155311]
8. Tummers QRJG, Verbeek FPR, Schaafsma BE, Boonstra MC, van der Vorst JR, Liefers GJ, van de Velde CJH, Frangioni JV, Vahrmeijer AL. Real-time intraoperative detection of breast cancer using

near-infrared fluorescence imaging and Methylene Blue. Eur J Surg Oncol. 2014; 40:850–858. [PubMed: 24862545]

9. Kosaka N, Mitsunaga M, Longmire MR, Choyke PL, Kobayashi H. Near infrared fluorescence-guided real-time endoscopic detection of peritoneal ovarian cancer nodules using intravenously injected indocyanine green. Int J Cancer. 2011; 129:1671–1677. [PubMed: 21469142]
10. Sheth RA, Arellano RS, Uppot RN, Samir AE, Goyal L, Zhu AX, Gervais DA, Mahmood U. Prospective trial with optical molecular imaging for percutaneous interventions in focal hepatic lesions. Radiology. 2015; 274:917–926. [PubMed: 25302707]
11. Weissleder R. Molecular imaging in cancer. Science. 2006; 312:1168–1171. [PubMed: 16728630]
12. vanDam GM, Themelis G, Crane LMA, Harlaar NJ, Pleijhuis RG, Kelder W, Sarantopoulos A, de Jong JS, Arts HJG, van der Zee AGJ, Bart J, Low PS, Ntziachristos V. Intraoperative tumor-specific fluorescence imaging in ovarian cancer by folate receptor-a targeting: First inhuman results. Nat Med. 2011; 17:1315–1319. [PubMed: 21926976]
13. Ardeshirpour Y, Hassan M, Zielinski R, Horton JA, Capala J, Gandjbakhche AH, Chernomordik V. In vivo assessment of HER2 receptor density in HER2-positive tumors by near-infrared imaging, using repeated injections of the fluorescent probe. Technol Cancer Res Treat. 2014; 13:427–434. [PubMed: 24000992]
14. Weissleder R, Tung CH, Mahmood U, Bogdanov A Jr. In vivo imaging of tumors with protease-activated near-infrared fluorescent probes. Nat Biotechnol. 1999; 17:375–378. [PubMed: 10207887]
15. Koblinski JE, Ahram M, Sloane BF. Unraveling the role of proteases in cancer. Clin Chim Acta. 2000; 291:113–135. [PubMed: 10675719]
16. Mohamed MM, Sloane BF. Cysteine cathepsins: Multifunctional enzymes in cancer. Nat Rev Cancer. 2006; 6:764–775. [PubMed: 16990854]
17. Mito JK, Ferrer JM, Brigman BE, Lee CL, Dodd RD, Eward WC, Marshall LF, Cuneo KC, Carter JE, Ramasunder S, Kim Y, Lee WD, Griffith LG, Bawendi MG, Kirsch DG. Intra-operative detection and removal of microscopic residual sarcoma using wide-field imaging. Cancer. 2012; 118:5320–5330. [PubMed: 22437667]
18. Bartholf DeWitt, S.; Eward, C.; Eward, WC.; Lazarides, AL.; Kirsch, DG.; Cardona, DM.; Brigman, BE.; Mito, JK.; Whitley, MJ.; Ferrer, JM.; Strasfeld, DB.; Lee, D.; Concannon, K.; Spodnick, G.; Holmes, E.; Miller, K.; Berg, J. The American College of Veterinary Surgeons 2014 Surgery Summitt. San Diego, California: 2014.
19. Freireich EJ, Gehan EA, Rall DP, Schmidt LH, Skipper HE. Quantitative comparison of toxicity of anticancer agents in mouse, rat, hamster, dog, monkey, and man. Cancer Chemother Rep. 1966; 50:219–244. [PubMed: 4957125]
20. O'Sullivan B, Davis AM, Turcotte R, Bell R, Catton C, Chabot P, Wunder J, Kandel R, Goddard K, Sadura A, Pater J, Zee B. Preoperative versus postoperative radiotherapy in soft-tissue sarcoma of the limbs: A randomised trial. Lancet. 2002; 359:2235–2241. [PubMed: 12103287]
21. Segal E, Prestwood TR, van der Linden WA, Carmi Y, Bhattacharya N, Withana N, Verdoes M, Habtezion A, Engleman EG, Bogyo M. Detection of intestinal cancer by local, topical application of a quenched fluorescence probe for cysteine cathepsins. Chem Biol. 2015; 22:148–158. [PubMed: 25579207]
22. Bremer C, Tung CH, Weissleder R. In vivo molecular target assessment of matrix metalloproteinase inhibition. Nat Med. 2001; 7:743–748. [PubMed: 11385514]
23. Olson ES, Jiang T, Aguilera TA, Nguyen QT, Ellies LG, Scadeng M, Tsien RY. Activatable cell penetrating peptides linked to nanoparticles as dual probes for in vivo fluorescence and MR imaging of proteases. Proc Natl Acad Sci USA. 2010; 107:4311–4316. [PubMed: 20160077]
24. Quillard T, Croce K, Jaffer FA, Weissleder R, Libby P. Molecular imaging of macrophage protease activity in cardiovascular inflammation in vivo. Thromb Haemost. 2011; 105:828–836. [PubMed: 21225096]
25. Lewis CE, Pollard JW. Distinct role of macrophages in different tumor microenvironments. Cancer Res. 2006; 66:605–612. [PubMed: 16423985]
26. Lin EY, Nguyen AV, Russell RG, Pollard JW. Colony-stimulating factor 1 promotes progression of mammary tumors to malignancy. J Exp Med. 2001; 193:727–740. [PubMed: 11257139]

27. Caldwell GW, Masucci JA, Yan Z, Hageman W. Allometric scaling of pharmacokinetic parameters in drug discovery: Can human CL, V_{ss} and $t_{1/2}$ be predicted from in-vivo rat data? Eur J Drug Metab Pharmacokinet. 2004; 29:133–143. [PubMed: 15230342]
28. Kolokotrones T, Van S, Deeds EJ, Fontana W. Curvature in metabolic scaling. Nature. 2010; 464:753–756. [PubMed: 20360740]
29. Caron WP, Clewell H, Dedrick R, Ramanathan RK, Davis WL, Yu N, Tonda M, Schellens JH, Beijnen JH, Zamboni WC. Allometric scaling of pegylated liposomal anticancer drugs. J Pharmacokinet Pharmacodyn. 2011; 38:653–669. [PubMed: 21863380]
30. Dupont WD, Plummer WD Jr. Power and sample size calculations. A review and computer program. Control Clin Trials. 1990; 11:116–128. [PubMed: 2161310]
31. Cuneo KC, Mito JK, Javid MP, Ferrer JM, Kim Y, Lee WD, Bawendi MG, Brigman BE, Kirsch DG. Imaging primary mouse sarcomas after radiation therapy using cathepsin-activatable fluorescent imaging agents. Int J Radiat Oncol Biol Phys. 2013; 86:136–142. [PubMed: 23391816]
32. Taylor, DL.; Wang, Y-l. Fluorescence microscopy of living cells in culture. In: Wilson, L., editor. Methods in Cell Biology. Vol. 29. Academic Press; San Diego, CA: 1989. p. 1-328.
33. Sachdeva M, Mito JK, Lee CL, Zhang M, Li Z, Dodd RD, Cason D, Luo L, Ma Y, Van Mater D, Gladdy R, Lev DC, Cardona DM, Kirsch DG. MicroRNA-182 drives metastasis of primary sarcomas by targeting multiple genes. J Clin Invest. 2014; 124:4305–4319. [PubMed: 25180607]
34. Jackson EL, Willis N, Mercer K, Bronson RT, Crowley D, Montoya R, Jacks T, Tuveson DA. Analysis of lung tumor initiation and progression using conditional expression of oncogenic *K*-ras. Genes Dev. 2001; 15:3243–3248. [PubMed: 11751630]
35. Dankort D, Filenova E, Collado M, Serrano M, Jones K, McMahon M. A new mouse model to explore the initiation, progression, and therapy of $BRAF^{V600E}$-induced lung tumors. Genes Dev. 2007; 21:379–384. [PubMed: 17299132]
36. Jonkers J, Meuwissen R, van der Gulden H, Peterse H, van der Valk M, Berns A. Synergistic tumor suppressor activity of BRCA2 and p53 in a conditional mouse model for breast cancer. Nat Genet. 2001; 29:418–425. [PubMed: 11694875]
37. Srinivas S, Watanabe T, Lin CS, William CM, Tanabe Y, Jessell TM, Costantini F. Cre reporter strains produced by targeted insertion of *EYFP* and *ECFP* into the *ROSA26* locus. BMC Dev Biol. 2001; 1:4. [PubMed: 11299042]
38. Kirsch DG, Dinulescu DM, Miller JB, Grimm J, Santiago PM, Young NP, Nielsen GP, Quade BJ, Chaber CJ, Schultz CP, Takeuchi O, Bronson RT, Crowley D, Korsmeyer SJ, Yoon SS, Hornicek FJ, Weissleder R, Jacks T. A spatially and temporally restricted mouse model of soft tissue sarcoma. Nat Med. 2007; 13:992–997. [PubMed: 17676052]
39. Huang Y, Yuan J, Righi E, Kamoun WS, Ancukiewicz M, Nezivar J, Santosuosso M, Martin JD, Martin MR, Vianello F, Leblanc P, Munn LL, Huang P, Duda DG, Fukumura D, Jain RK, Poznansky MC. Vascular normalizing doses of antiangiogenic treatment reprogram the immunosuppressive tumor microenvironment and enhance immunotherapy. Proc Natl Acad Sci USA. 2012; 109:17561–17566. [PubMed: 23045683]
40. Ager EI, Kozin SV, Kirkpatrick ND, Seano G, Kodack DP, Askoxylakis V, Huang Y, Goel S, Snuderl M, Muzikansky A, Finkelstein DM, Dransfield DT, Devy L, Boucher Y, Fukumura D, Jain RK. Blockade of MMP14 activity in murine breast carcinomas: Implications for macrophages, vessels, and radiotherapy. J Natl Cancer Inst. 2015; 107:djv017. [PubMed: 25710962]

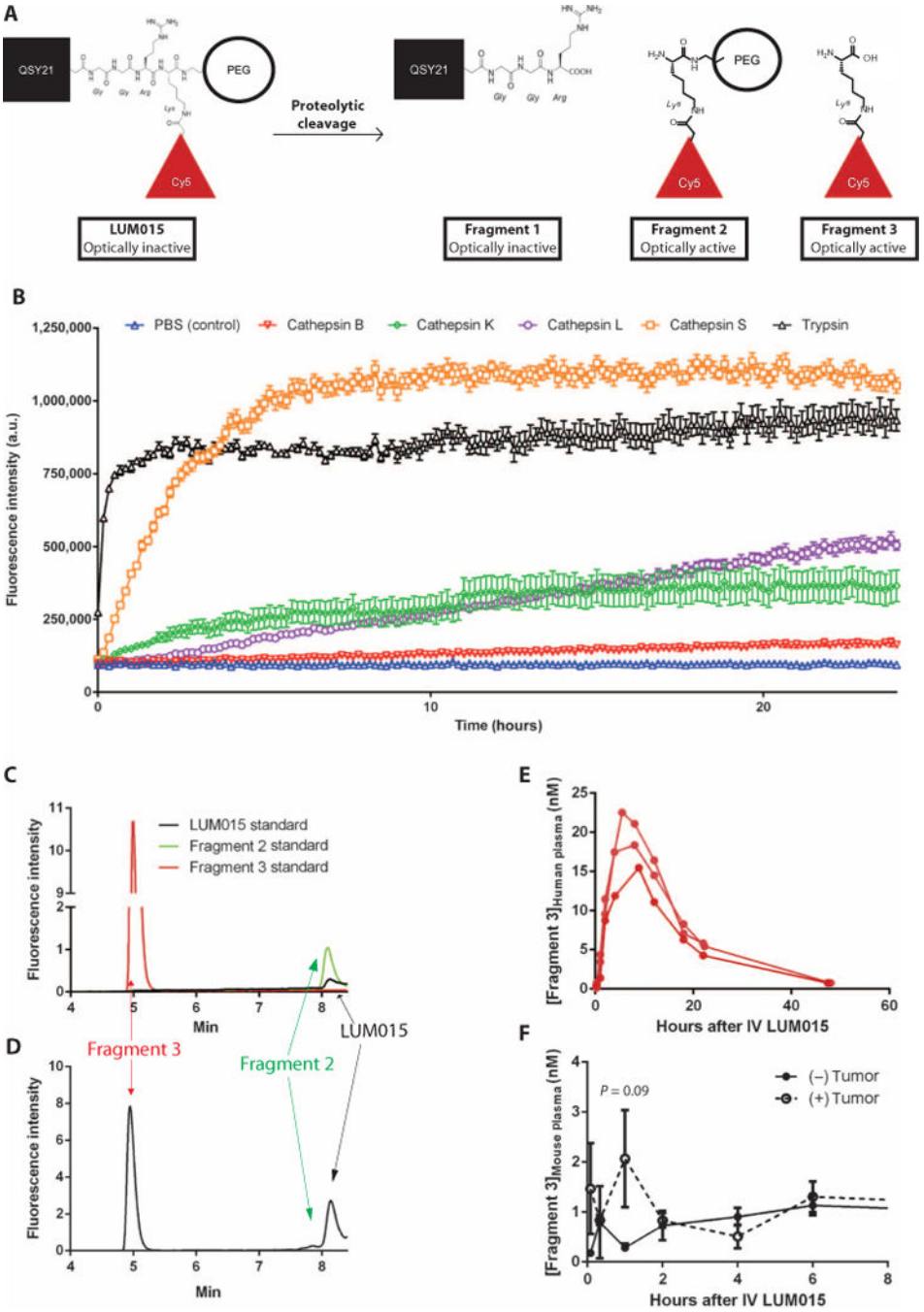

Fig. 1. Cy5-Lys is the major fluorescent LUM015 metabolite

(**A**) Expected LUM015 cleavage products: Fragment 1 contains the quencher QSY21, and optically active fragments 2 and 3 contain the Cy5 fluorophore. (**B**) In vitro protease (0.5 μM) activation of LUM015 (5 μM). Fluorescence was measured at multiple time points with peak excitation at 650 nm and fluorescence emission collection at 675 nm (n = 6 replicates per enzyme). (**C** and **D**) HPLC analysis of pure LUM015 (25 ng/ml), fragment 2 (25 ng/ml), and fragment 3 (2.5 ng/ml) (C) and a representative patient plasma sample collected from patient 14 at 8 hours after intravenous administration of LUM015 (1.5 mg/kg) (D). (**E** and

F) Plasma profiles of fragment 3 in three patients (E) and in tumor-bearing and non–tumor-bearing mice (n = 6 mice per group) (F) each injected with LUM015 (1.5 mg/kg). P value determined by unpaired t test.

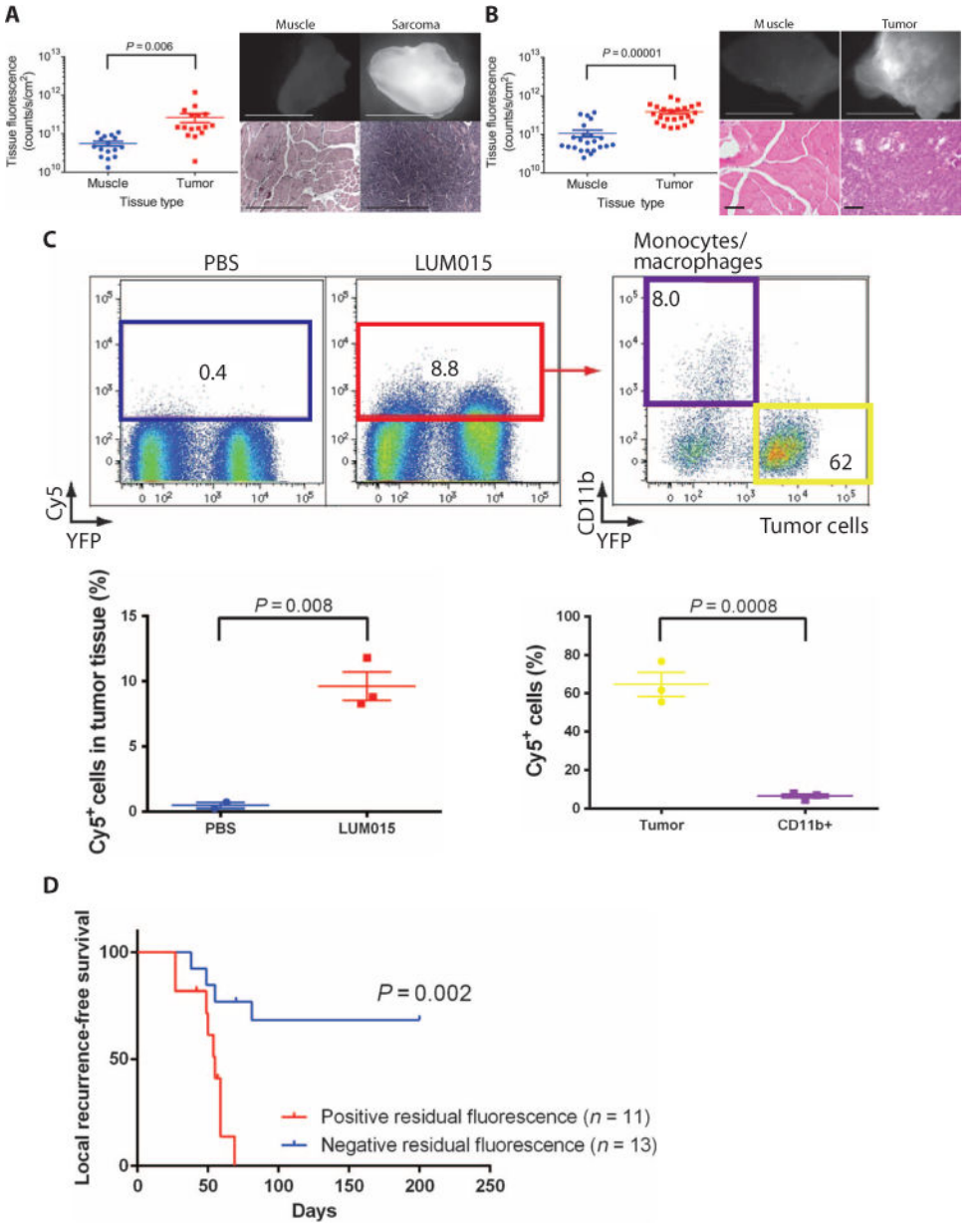

Fig. 2. LUM015 fluorescently labels tumor cells in mouse models of STS and breast cancer

(**A** and **B**) Mean measured fluorescence in primary sarcoma (n = 16) (A) or orthotopic breast cancer (n = 23) (B) and muscle. P values determined by unpaired t test. Representative fluorescence images of resected normal muscle and tumors are shown along with corresponding hematoxylin and eosin (H&E) histology. The same contrast scale was applied to both fluorescence images in each pair. Scale bars, 5 mm for fluorescence images; 500 μm for H&E images in (A); 100 μm for H&E images in (B). (**C**) Representative flow cytometric analysis of resected mouse tumors expressing tumor cell–specific YFP after intravenous administration of phosphate-buffered saline (PBS) or LUM015 (3.5 mg/kg). Of the tumors from mice treated with LUM015, $Cy5^+$ cells (red box, cells with fluorescence >2 × 10^2) and YFP^+ tumor cells (yellow box) were sorted and quantified (n_{PBS} = 2 mice, n_{LUM015} = 3

mice). In the $Cy5^+$ cells, the proportions of YFP^+ tumor cells and $CD11b^+$ tumor–associated macrophages were further quantified (n = 3 mice). P values were determined by unpaired t test. (**D**) The correlation between residual fluorescence within the sarcoma tumor bed measured before wound closure and local recurrence–free survival in mice. P value determined by log-rank test.

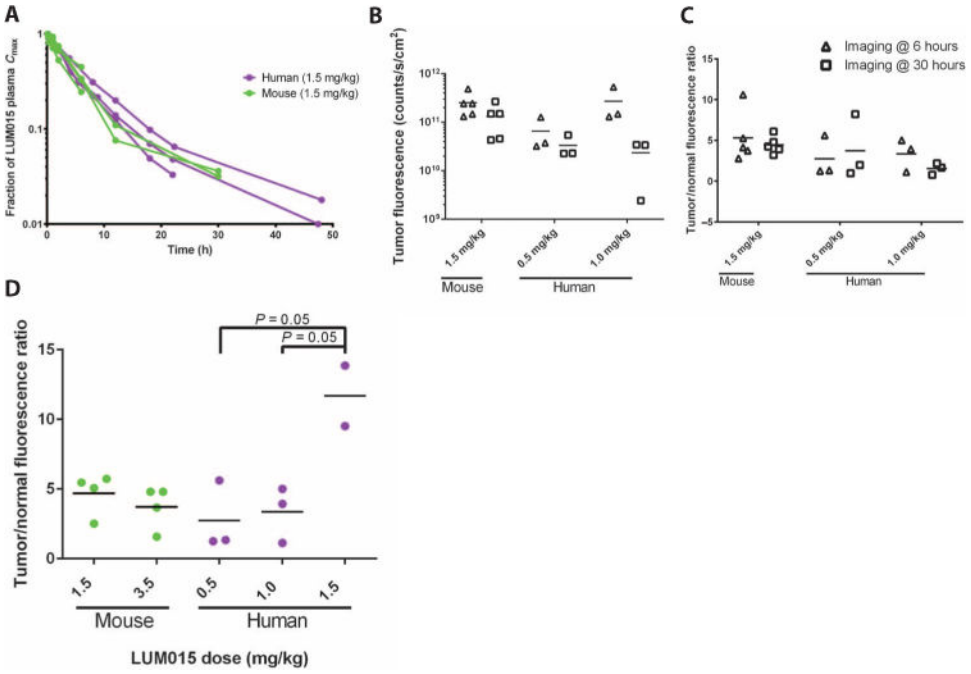

Fig. 3. Comparative LUM015 pharmacokinetics in mouse and human subjects

(**A**) LUM015 plasma clearance profile in mouse and human subjects administered a 1.5 mg/kg dose of LUM015. $[LUM015]_{plasma}$ is given as a fraction of the maximum concentration and shown on a log scale. (**B**) Tumor fluorescence in patients and mice at the 6- and 30-hour imaging time points (n = 5 mice and 3 humans per dose cohort). P = 0.02 for imaging time, as determined by two-way analysis of variance (ANOVA). (**C**) Tumor/normal fluorescence ratio in mice and humans at the 6- and 30-hour imaging time points. P = 0.6 for imaging time, as determined by two-way ANOVA. (**D**) Tumor/normal fluorescence ratio measured in humans and mice by dose ($n_{mouse\text{-}1.5,\ 3.5}$ = 5; $n_{human\text{-}0.5,\ 1.0}$ = 3; $n_{human\text{-}1.5}$ = 2). P values for dose cohort comparisons determined by Tukey's multiple comparisons test. P = 0.02 for dose effect on human subset determined by one-way ANOVA.

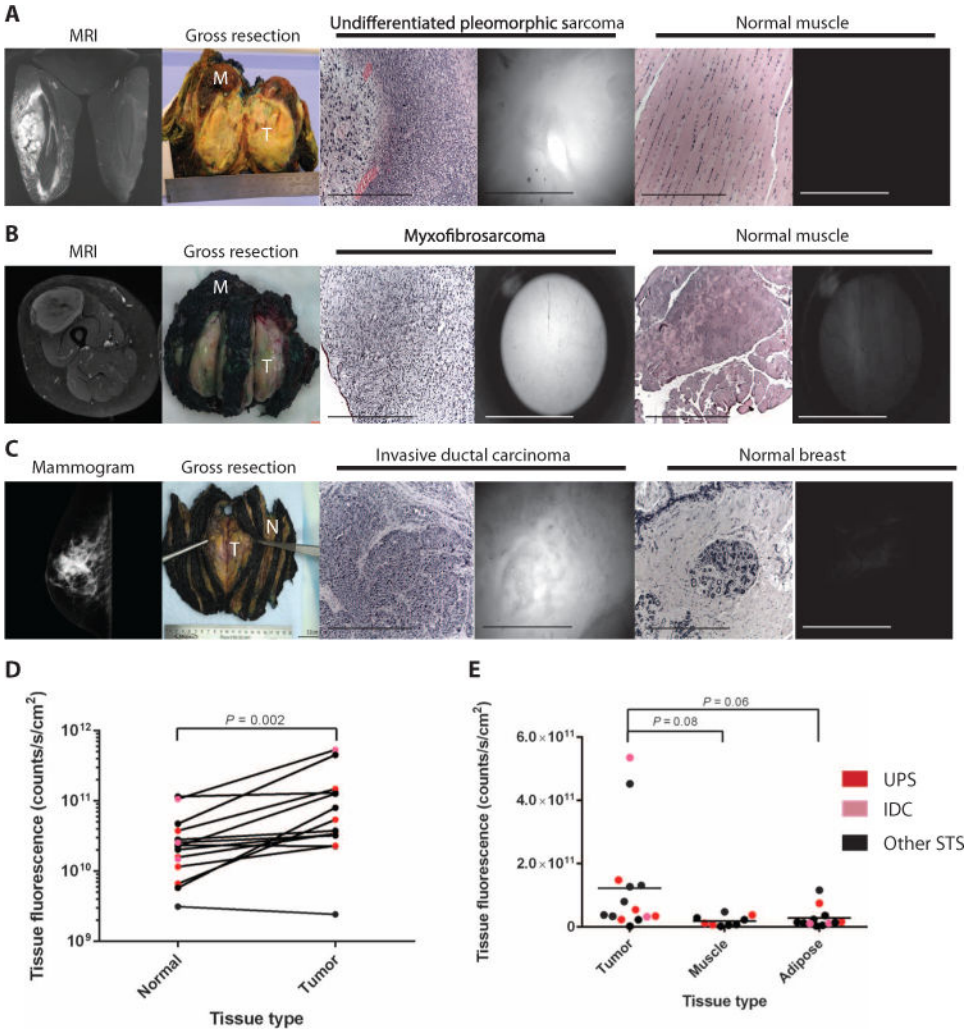

Fig. 4. Tumor-selective fluorescence in patients receiving intravenous LUM015 before resection

(**A** to **C**) Representative human subjects with UPS of the thigh (A, patient 2), myxofibrosarcoma of the thigh (B, patient 12), and IDC of the breast (C, patient 9). From left to right: gadolinium-enhanced magnetic resonance imaging, gross tissue resection containing tumor (T) and normal muscle (M), H&E histology of imaged tumor tissue, fluorescence image of tumor tissue obtained with the LUM device, H&E staining of imaged muscle, fluorescence image of muscle obtained with the LUM device. (**D**) Tumor tissue fluorescence and fluorescence measured from adjacent normal tissue in the same patient (n = 14). P value determined by paired t test. (**E**) Distribution of tumor, muscle, and adipose tissue fluorescence across all patients (n_{tumor} = 14, n_{muscle} = 10, $n_{adipose}$ = 11). P = 0.04 for tissue type effect determined by one-way ANOVA. P values for tumor to muscle and adipose comparison determined by unpaired t test.

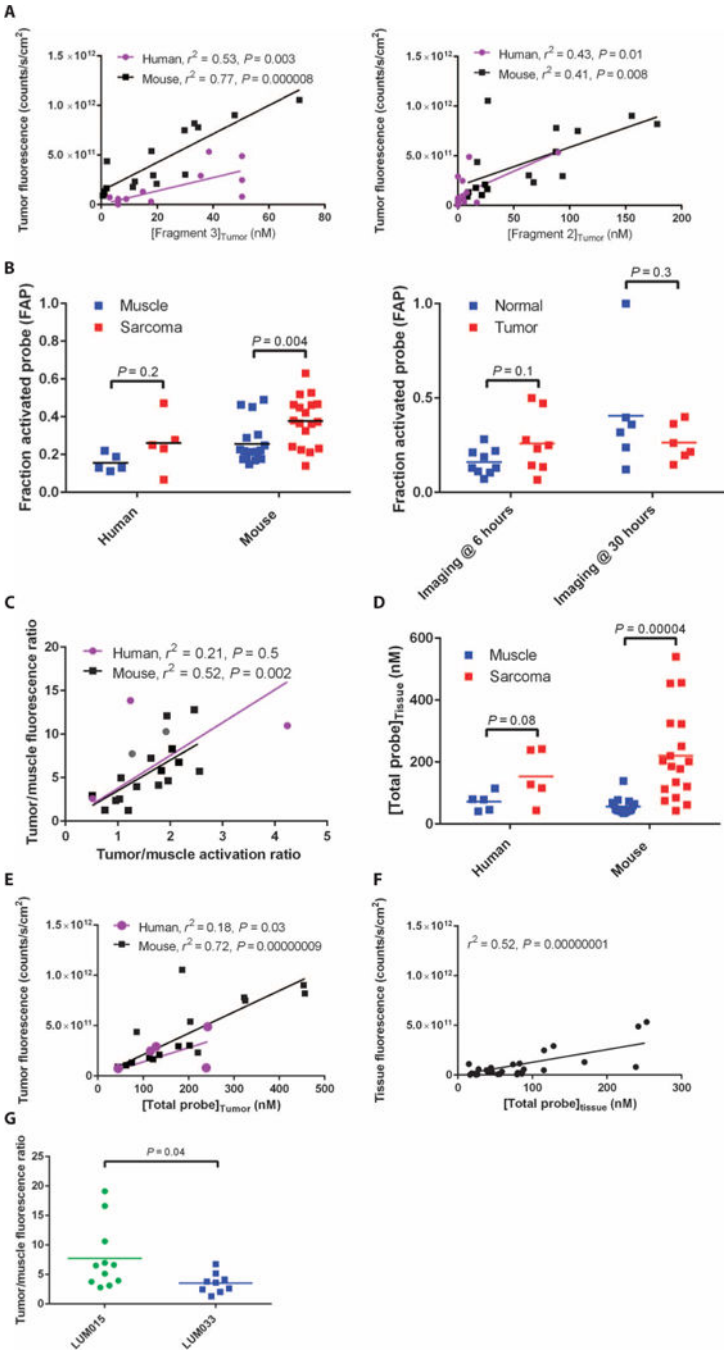

Fig. 5. Tumor-selective distribution and activation of LUM015

(**A**) Tumor fluorescence as a function of $[\text{fragment 3}]_{\text{tumor}}$ and $[\text{fragment 2}]_{\text{tumor}}$ (n_{human} = 14, n_{mouse} = 16). *P* values determined by *F* test on the linear regression model. (**B**) The FAP was determined using the following equation: $([\text{fragment 2 (nM)}]_{\text{tissue}} + [\text{fragment 3 (nM)}]_{\text{tissue}})/([\text{LUM015 (nM)}]_{\text{tissue}} + [\text{fragment 2 (nM)}]_{\text{tissue}} + [\text{fragment 3 (nM)}]_{\text{tissue}})$. FAP data are shown for muscle and tumor tissue samples from human (*n* = 5, patients 8 and 11 to 14) and mouse (*n* = 18) STS subjects and from all human subjects imaged at 6 and 30 hours (*n* = 14). *P* values determined by unpaired *t* test. (**C**) Correlation between the tumor: muscle

fluorescence ratio and the FAP ratio in the mouse and human STS cohorts (n_{human} = 5, n_{mouse} = 16). *P* value determined by *F* test on the linear regression model. (**D**) The [TP] in the tissue (in nM) was determined using the following equation: $[LUM015]_{tissue}$ + $[fragment\ 2]_{tissue}$ + $[fragment\ 3]_{tissue}$. [TP] data are shown for muscle and tumor tissue samples from human (*n* = 5, patients 8 and 11 to 14) and mouse (*n* = 18) STS subjects. *P* values determined by unpaired *t* test. (**E** and **F**) Tumor fluorescence versus [TP] in the mouse and human STS cohorts (n_{human} = 5, n_{mouse} = 16) (E) and in tumor and normal tissue samples from all human subjects (*n* = 14 per tissue type) (F). *P* values determined by *F* test on the linear regression models. (**G**) Tumor/muscle fluorescence ratios measured in mice 6 hours after injection with equimolar amounts of LUM015 or LUM033 (n_{LUM015} = 11, n_{LUM033} = 9). *P* value determined by unpaired *t* test.

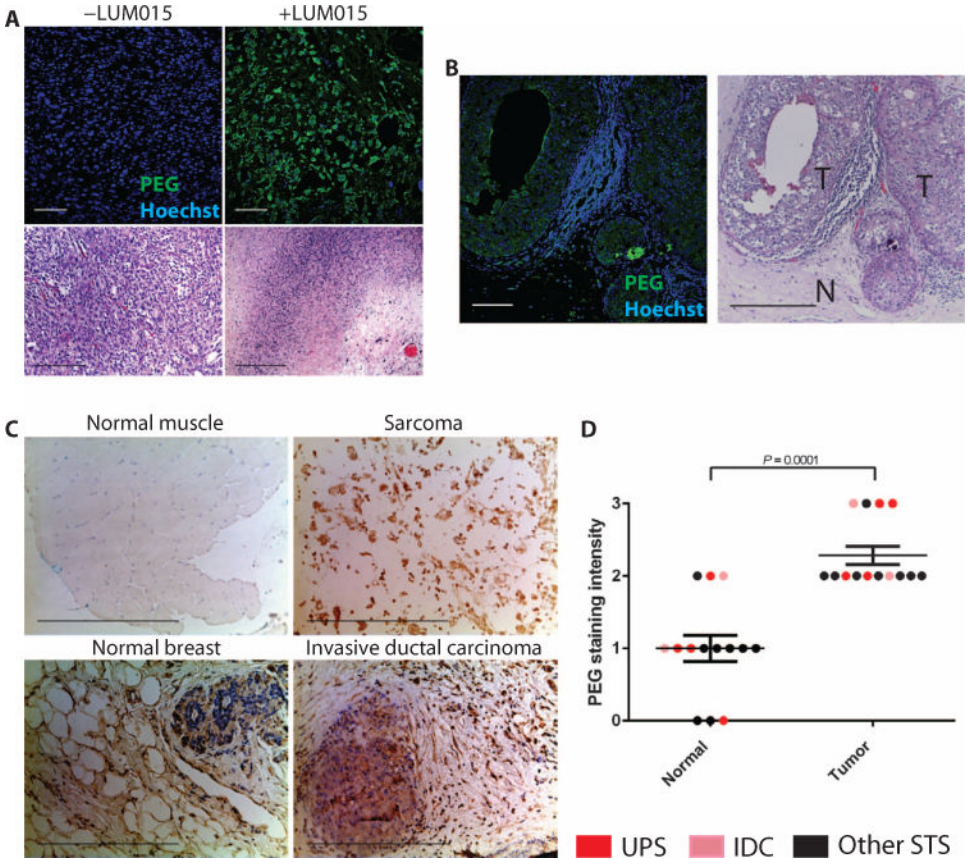

Fig. 6. Visualizing tumor-selective LUM015 biodistribution

(**A**) PEG immunofluorescence of human tumor samples from LUM015-injected patients (+LUM015 representative image from patient 2) and from uninjected patients (−LUM015 representative image from *n* = 3 patients) with UPS. (**B**) PEG immunofluorescence of margin tissue from LUM015-injected breast cancer patient 15. T, tumor tissue; N, normal breast tissue. The corresponding H&E histology is shown. (**C**) Immunohistochemistry for PEG in normal muscle tissue, normal breast tissue, and tumor tissue. Representative images of normal muscle and UPS (patient 2) as well as normal breast and IDC (patient 9). (**D**) Quantification of PEG staining intensity in tumors and normal tissues (*n* = 14 per tissue type; 1 tumor and 1 normal tissue sample from each patient except patient 10). *P* value determined by Mann-Whitney test.

Table 1

Enrolled patients in first-in-human phase 1 clinical trial of LUM015

Imaging time was measured as the number of hours elapsed between LUM015 injection and imaging of the resected tissues with the LUM device. Histological descriptors are based on clinical surgical pathology reports. ER, estrogen receptor; PR, progesterone receptor; RT, radiation therapy.

Patient	LUM015 dose (mg/kg)	Imaging time (hours)	Tumor type	Tumor grade	Tumor volume (cm^3)	Neoadjuvant therapy	Tumor site
1	0.5	30.1	Well-differentiated liposarcoma	Low	10.5 × 8.5 × 6.2	None	Retroperitoneal
2	0.5	28.5	UPS	High	13.5 × 8.3 × 6.5	25 × 2 Gy RT	Thigh
3	0.5	28.5	UPS	High	18.0 × 9.0 × 6.0	25 × 2 Gy RT	Upper arm
4	1.0	30.9	Malignant peripheral nerve sheath tumor	Intermediate	2.5 × 1.6 × 1.5	25 × 2 Gy RT	Upper arm
5	1.0	26.9	Myxoinflammatory fibroblastic sarcoma/ hemosiderotic fibrolipomatous tumor	Low	31.0 × 20.0 × 1.3	None	Leg
6	1.0	26.5	UPS	High	3.6 × 2.9 × 1.2	None	Upper arm
7	1.0	4.8	Metastatic clear cell sarcoma	High	4.0 × 2.9 × 2.8	None	Inguinal lymph node
8	1.0	7.2	UPS	High	13.0 × 6.5 × 7.1	25 × 2 Gy RT	Upper arm
9	1.0	8.3	IDC: $ER^+/PR^-/Her2^+$	High	3.7	None	Breast
10	1.5	9.6	IDC: $ER^+/PR^+/Her2^-$	Intermediate	7.5 × 2.5 ×1.5	None	Breast
11	1.5	5.1	Metastatic spindle cell sarcoma	Low	0.9	None	Thigh
12	1.5	7.3	Myxofibrosarcoma	High	11.0 × 6.5 × 6.5	None	Thigh
13	0.5	9.6	Synovial sarcoma	High	20.0 × 12.0 × 6.0	25 × 2 Gy RT	Thigh
14	0.5	8.5	Spindle cell sarcoma	High	7.5	25 × 2 Gy RT	Thigh
15	0.5	7.3	IDC: ER^+, PR^+, $Her2^-$	High	2.4 × 1.6 × 1.4	None	Breast